PHYSICAL REVIEW B **89**, 085130 (2014)

Electronic structure of $Ba_3CuSb_2O_9$: A candidate quantum spin liquid compound

K. V. Shanavas,[*] Z. S. Popović,[†] and S. Satpathy

Department of Physics & Astronomy, University of Missouri, Columbia, Missouri 65211, USA

(Received 26 December 2012; revised manuscript received 21 December 2013; published 27 February 2014)

Using density-functional methods, we study the electronic structure of $Ba_3CuSb_2O_9$, a candidate material for the quantum spin liquid behavior. We study both the triangular lattice as well as the recently proposed hexagonal lattice structures with flipped Cu-Sb dumbbells. The band structure near the Fermi energy is described very well by a tight-binding Hamiltonian involving the Cu (e_g) orbitals, confirming their central role in the physics of the problem. A minimal tight-binding Hamiltonian for the triangular structure is presented. The Cu (d^9) ions (a single e_g hole in the band structure) present in the compound are expected to be Jahn-Teller centers, while the nature of the Jahn-Teller distortions in this material is still under debate. Solving a simple model by exact diagonalization, we show that electronic correlation effects in general enhance the tendency towards a Jahn-Teller distortion by reducing the kinetic energy due to correlation effects. Our density-functional calculations do indeed show a significant Jahn-Teller distortion of the CuO_6 octahedra when we include the correlation effects within the Coulomb-corrected GGA+U method, so that the Jahn-Teller effect is correlation driven. We argue for the presence of a random static Jahn-Teller distortion in the hexagonal structure rather than a dynamical one because of the broken octahedral symmetry around the CuO_6 octahedra and the potential fluctuations inherently present in the system caused by a significant disorder, which is believed to be present, in particular, due to the flipped Cu-Sb dumbbells.

DOI: 10.1103/PhysRevB.89.085130 PACS number(s): 75.10.Kt, 71.15.Mb, 71.70.Ej, 75.47.Lx

I. INTRODUCTION

Geometrically frustrated magnets are of considerable current interest owing to the novel magnetic ground states that they might possess [1,2]. Frustration leads to a massively degenerate ground state, which has been observed in the spin ice systems such as $Dy_2Ti_2O_7$ [3], where the massive degeneracy manifests itself as a finite entropy at zero temperature. Analogous to the water ice system studied long ago by Pauling [4,5], the classical spin ice systems are characterized by large magnetic moments so that the fluctuations stop as temperature is lowered, with the system eventually settling down into the massively degenerate ground state with a finite entropy. It has been suggested that if the spin is small (e.g., $S = 1/2$ or 1), the zero-point quantum fluctuations may remain even at $T = 0$, resulting in a quantum spin liquid state. Such a state would be characterized as nonmagnetic, though with well-formed local moments, which are in addition entangled with one another over long distances [2]. Even though the original proposal of Anderson [6] about the existence of the quantum spin liquid state was made as early as 1973, the discovery of it in real materials has remained elusive, even though its classical counterpart, the spin ice state, has now been established in several systems.

Recently, $Ba_3CuSb_2O_9$ has been proposed as a possible candidate for the quantum spin liquid state, since in addition to the essential requirements of the small spin and frustration, it shows a linear-T specific heat behavior and no magnetic order, both characteristics of the spin liquid state [4,7,8]. The Cu $S = 1/2$ state, responsible for the low spin of the system, indicates a Cu (d^9) configuration with degenerate electron states coupled to the lattice via the Jahn-Teller (JT) interaction. However, the lack of a static JT distortion in the compound has been a puzzling issue for quite some time and in fact a recent paper has suggested that the JT effect may be dynamic, so that a static distortion is not observed [9]. Other authors have suggested a random static JT distortion in the compound, where the distortion axes of the individual CuO_6 octahedra are oriented randomly due to disorder.

To address these issues and to understand the nature of the electron states in general, we study here the electronic structure of $Ba_3CuSb_2O_9$ both in the triangular and the recently proposed hexagonal structure by performing density-functional calculations. Even though the material currently exists in the hexagonal structure, we present our studies for both triangular and hexagonal structures in this paper, since there is an ongoing attempt [10] to synthesize it in the triangular structure as well, e.g., growing under an applied electric field (which may suppress the flipping of the Cu-Sb dipoles resulting in the triangular structure). Our method included the exchange-correlation functional within the generalized gradient approximation (GGA) and its Coulomb corrected version (GGA+U) as well. We find that the band structure near the Fermi energy, which consists of Cu (e_g) states, may be described by an effective Cu (e_g) Hamiltonian, obtained by folding in the effects of the other orbitals via the Löwdin perturbation; the form of the Hamiltonian is explicitly given for the triangular case.

An insulating solution is obtained from the GGA+U calculations. Within the GGA, we find no JT distortion of the CuO_6 octahedra, which is suppressed due to a relatively strong kinetic energy as compared to the strength of the JT interaction. As is well known, the Coulomb correlation reduces the kinetic energy in general, so that a JT distortion becomes more favorable as the JT-suppressing kinetic energy becomes weaker. We illustrate this with the exact diagonalization of a simple model for a single Cu hexagon. Indeed, the GGA+U

---

[*] shanavasv@missouri.edu

[†] Permanent address: Institute of Nuclear Sciences, Vinča, University of Belgrade, P. O. Box 522, 11001 Belgrade, Serbia.

results for the triangular lattice do indicate presence of a JT distortion. For the hexagonal lattice, the crystal structure is such that the symmetry axes of the individual CuO_6 octahedra are oriented in different directions. We argue that this together with lattice disorder due to disordered flipped Cu-Sb dumbbells makes a random static JT distortion more likely in the system rather than a dynamical JT effect. This is consistent with the random static JT distortions suggested from several experiments.

The paper is organized as follows. We begin with a discussion of the crystal structure both for the triangular and the hexagonal lattices in Sec. II, followed by the density-functional electronic structure for both cases in Sec. III. An effective tight-binding 2×2 Hamiltonian for the Cu e_g states, which are the important states at the Fermi energy, is given in Sec. III A [Eqs. (5) and (6)] after including the effects of the O-p orbitals via the Löwdin downfolding procedure. We propose that this effective 2×2 Hamiltonian together with a Hubbard U term and an appropriate $E \otimes e$ Jahn-Teller coupling term [11,12], discussed in Sec. IV A 2, is a minimal model for the description of the electronic structure for the triangular lattice. A similar minimal Hamiltonian for the hexagonal lattice may be obtained following the procedure in Sec. III A, but its explicit form is not given here.

Section IV is devoted to a discussion of the Jahn-Teller effect. No Jahn-Teller distortion is found from the density-functional structure optimization with the GGA functional without the Coulomb U correction, while the GGA+U calculations yield a finite Jahn-Teller distortion and subsequently lead to an insulating solution. Section IV A illustrates the tendency of the kinetic energy to suppress the Jahn-Teller distortion by considering (i) a simple two-site model and (ii) the triangular lattice relevant for the present case. Next in Sec. IV B we make an important point that electronic correlation effects enhance the tendency towards the Jahn-Teller distortion, in essence by suppressing the kinetic energy. This is illustrated by exactly solving a model many-body Hamiltonian for a single hexagon with and without a Hubbard U term using exact diagonalization. Density-functional results for the present compound with the GGA+U functional, which takes into account the correlation effects within the density-functional theory, are presented in Sec. IV C. In Sec. IV D we argue for a static but random Jahn-Teller distortion in the system rather than a dynamical Jahn-Teller effect, both of which have been debated in the literature. Finally, some concluding remarks are made in the summary, Sec. V.

II. CRYSTAL STRUCTURE

There are two different crystal structures for $Ba_3CuSb_2O_9$ proposed in the literature [7,13], which are closely related to each other and we consider both in this paper. The first structure, proposed quite early on by Köhl [7], has triangular layers of Cu atoms, which are well separated by intervening layers of the remaining types of atoms. The crystal structure is made up of a framework consisting of corner-sharing SbO_6 octahedra and face-sharing $CuSbO_9$ bioctahedra. The middle layer of the three O atoms within the bioctahedra are connected to the Cu and the Sb atom forming the CuO_3Sb dumbbells (we call these the Cu-Sb dumbbells in the rest of the paper). The Cu ions occupy the $2b$ Wyckoff site of space group $P6_3mc$, and this site forms the triangular lattice in the ab plane (Fig. 1). The structure can be seen as two-dimensional magnetic layers of Cu atoms organized on a triangular lattice, with the layers separated by intervening layers of nonmagnetic atoms (Fig. 2).

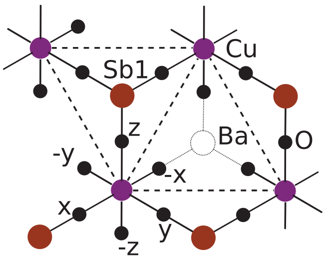

FIG. 1. (Color online) A single plane of Cu in the triangular lattice structure, showing the dominant electron hopping paths Cu-O-Sb-O-Cu. The corners of three neighboring CuO_6 octahedra are connected via an Sb atom, which lies above the center of the triangle. Shown also are the local coordinate axes for one of the Cu atoms used to define the local Cu (e_g) orbitals, which form the bands near the Fermi energy. All Sb atoms shown here occur on a plane above the Cu layer and are labeled Sb1, while a second set of Sb atoms, labeled Sb2 and not shown here, occurs directly below the Cu atoms, connected to the Cu through three O atoms, indicated by $-x$, $-y$, and $-z$, forming the CuO_3Sb "dumbbell" (see Fig. 2). In the hexagonal structure, a third of these dumbbells are flipped by interchanging Cu and Sb2, so that the remaining two-thirds of the Cu atoms in the plane form a hexagonal lattice. A less important hopping path consists of Cu-O-Ba-O-Cu, with the Ba atom connected to the O atoms below the plane in a manner similar to the Sb atoms as indicated in the figure.

According to the more recent results of Nakatsuji *et al.* [13], the crystal structure is hexagonal with the space group $P6_3/mmc$. This structure, illustrated in Fig. 3, is derived

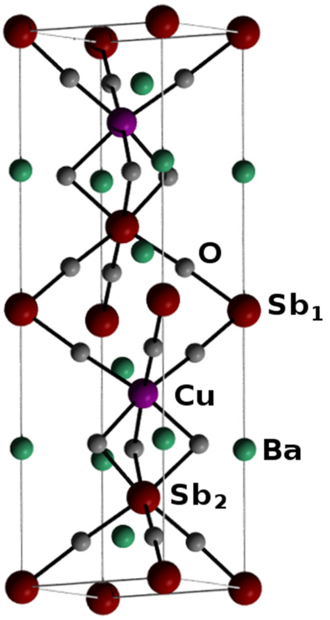

FIG. 2. (Color online) Crystallographic unit cell of $Ba_3CuSb_2O_9$ in the triangular lattice structure.

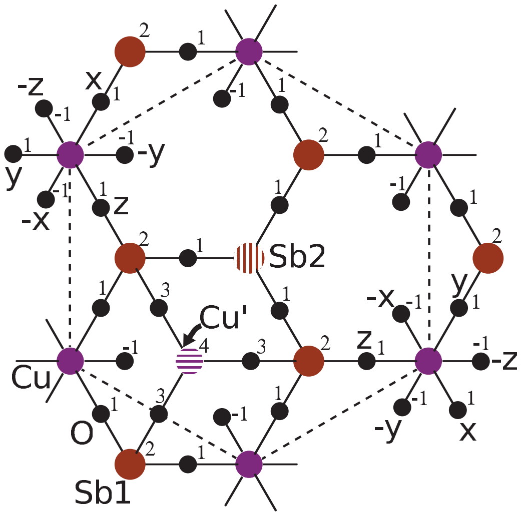

FIG. 3. (Color online) The hexagonal structure, which is obtained from the triangular structure of Fig. 1 by inverting a third of the Cu-Sb dumbbells as discussed in the text. The hatched Cu′ and Sb atoms are the results of the dumbbell inversions (interchange of Cu and Sb in the dumbbell). The hatched Sb came from two layers directly below it and took the place of a Cu atom, spoiling the triangular lattice, while the Cu atom that was present there descended two layers below as a result of the dumbbell inversion. The numbers next to the atoms indicate the consecutive layer numbers above the hexagonal Cu plane (atoms in this plane are unnumbered). Two consecutive Cu hexagonal planes are six layers apart, but shifted with respect to one another such that the next hexagonal layer Cu atom occurs directly above Cu′.

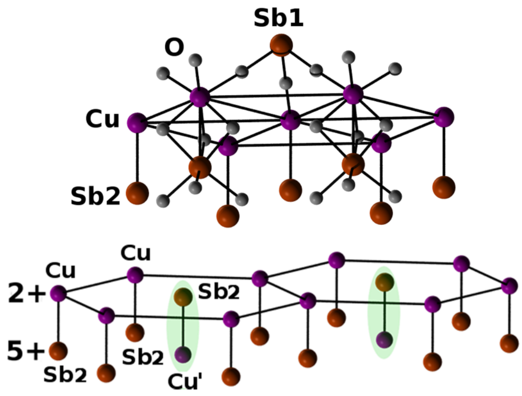

FIG. 4. (Color online) A Cu plane in the triangular lattice structure (*top*) and the interchange of the Cu-Sb2 atoms, highlighted in green, in the hexagonal lattice structure (*bottom*). In the latter, two-thirds of the Cu atoms in the original triangular lattice structure remain on the plane, while a third of the Cu atoms move out of the plane as shown in the bottom figure.

from the triangular structure by taking a third of the Cu-Sb dumbbells and interchanging the Cu and Sb atoms, so that the remaining Cu atoms in the plane form a hexagonal lattice instead of the original triangular lattice. A rationale for this structure is that since each dumbbell carries an electric dipole moment caused by the charge difference between $\mathrm{Cu^{2+}}$ and $\mathrm{Sb^{5+}}$, the electrostatic energy is minimized if the neighboring dipoles are aligned antiparallel to one another to the extent possible. In fact, from our density-functional calculations with the GGA, we do find that the hexagonal structure is energetically favorable over the triangular structure by an energy of 0.1 eV per $\mathrm{Ba_3CuSb_2O_9}$ formula unit. In the hexagonal structure, two-thirds of these dipoles are aligned along the c axis, while the remaining one-third are aligned antiparallel to them, as a result of the dumbbell inversion (Fig. 4). Note that the triangular structure has two formula units $(\mathrm{Ba_3CuSb_2O_9})_2$ in the crystalline unit cell, while the hexagonal structure has six.

The interchange of the Sb and Cu atoms in the hexagonal structure also modifies the electronic hopping paths. The Cu atoms that move out of the plane (Cu′ in Fig. 3) no longer participate in mediating exchange interactions between the Cu atoms on the hexagonal plane, as they have a much longer exchange path. There is a Cu′ atom (not shown in the figure) two layers directly below the hatched Sb atom as a result of the dumbbell inversion. The Cu′ atom shown in the figure is four layers above the hexagonal plane and came there as a result of the Cu-Sb interchange occurring in the next higher Cu hexagonal plane, six layers above the Cu plane shown in the figure. The Cu′ atoms spoil the symmetry of the hexagonal structure and in addition introduce new hopping paths between the Cu atoms, while destroying some old ones.

III. ELECTRONIC STRUCTURE

The first-principles density-functional theory (DFT) calculations presented here were performed using the Vienna *ab initio* simulation package (VASP) [14], which uses the projector augmented wave method. We used the generalized gradient approximation (GGA) to the exchange-correlation functional [15] or the Coulomb-corrected [16] GGA+U functional, a plane wave energy cutoff of 500 eV, and a **k**-space sampling on a $12 \times 12 \times 12$ Monkhorst-Pack grid for the Brillouin zone integrations for the triangular structure and a $4 \times 4 \times 4$ grid for the hexagonal structure. All calculations are for the spin-polarized ferromagnetic structure. All necessary structural relaxations are carried out until the Hellman-Feynman forces became less than 0.01 eV/Å. We also used two other all electron methods, viz., the linear muffin-tin orbitals (LMTO) and the linear augmented plane waves (LAPW) methods, to examine various aspects of the problem. All methods yielded essentially the same results. Unless otherwise stated, the DFT results presented here were obtained by using the VASP.

A. Band structure for the triangular lattice

We first discuss the electronic structure of the triangular lattice, which is the simpler lattice of the two and in terms of which the electronic structure of the hexagonal lattice may be understood. As discussed above, the hexagonal crystal structure is derived from the triangular structure by inverting a fraction of the Cu-Sb dumbbells. The calculated density of states (DOS) for the triangular structure is shown in Fig. 5. The electronic structure is consistent with the expected nominal chemical formula $\mathrm{Ba_3^{2+}Cu^{2+}Sb_2^{5+}O_9^{2-}}$, with the O $(2p)$ bands full and a single hole in the Cu $(3d)$ bands (Fig. 6), specifically in the minority-spin e_g band, indicated by $e_g^2 \downarrow$ in the middle

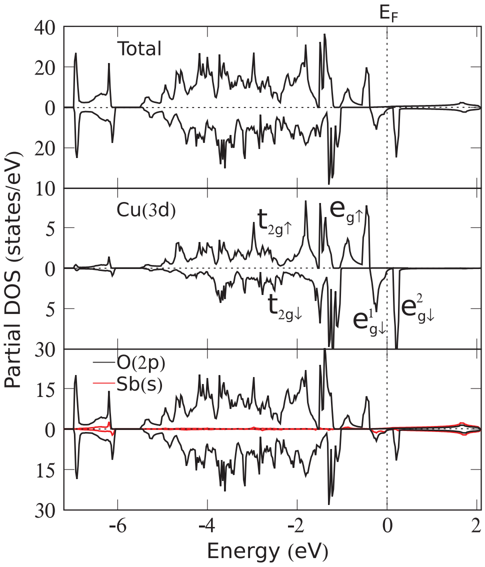

FIG. 5. (Color online) Spin-polarized total and partial density of states for the triangular structure, obtained from GGA calculations, indicating the Cu (e_g) ↓ hole. Defining the e_g orbitals with respect to the local coordinates pointed towards the neighboring oxygen atoms, the e_g and t_{2g} states are completely separated, allowing the band structure near E_F to be described in terms of an e_g Hamiltonian. In this basis, the $x^2 - y^2$ and the z^2 partial densities of states are identical. Hybridization of Cu (e_g) with the Sb (s) and O (p) states is seen due to the Cu-O-Sb-O-Cu hopping paths indicated in Fig. 1.

panel of Fig. 5. The Cu (t_{2g}) and e_g bands are clearly separated, with the t_{2g} bands overlapping with the top of the oxygen bands.

Quite remarkably, the e_g bands, which are the most important bands in the compound, are split into a lower e_g^1 band and an upper e_g^2 band due to the electronic hopping effects, even when there is no JT distortion as in the GGA results (Fig. 7). This splitting is further enhanced in the GGA+U calculation (see Fig. 8), where the structural optimization leads to a nonzero JT distortion. Each of these subbands splits further in the hexagonal structure due to the higher complexity of the latter structure. The e_g^1 and e_g^2 peaks seen in the DOS obtained with the GGA cannot simply be thought of as $x^2 - y^2$ and z^2 bands, as might have been the case if a strong JT distortion was present. In fact, each of these two e_g peaks is an equal mixture of the $x^2 - y^2$ and z^2 orbitals, as indicated from the top panel of Fig. 9, where the two partial DOS lie exactly on top of each other and are not distinguishable as two lines. The double-peaked structure comes from the special orientation of the CuO$_6$ octahedra as well as the characteristic Cu-Cu hopping path in the compound, rather than from a JT splitting. This will be more clear when we discuss below the tight-binding band structure.

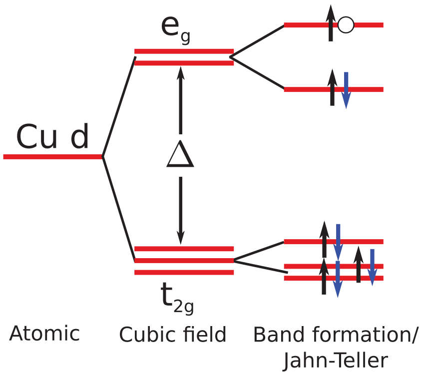

FIG. 6. (Color online) Cu (d^9) configuration with a single e_g ↓ hole as obtained from the DFT calculations both for the triangular and the hexagonal lattice structures.

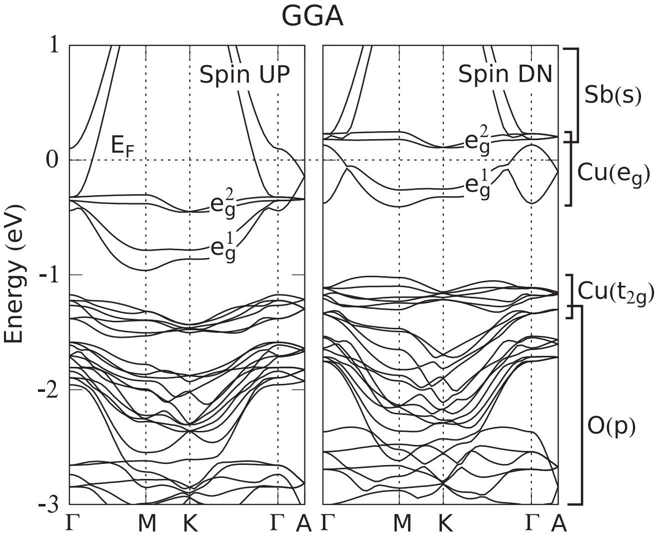

FIG. 7. Spin-polarized GGA band structure for the triangular structure indicating the dominant contribution of the Cu (e_g) states near the Fermi energy ($E_F = 0$) and the presence of the Cu (e_g) ↓ hole. Here the JT distortion is zero, as obtained from the structural optimization with the GGA functional.

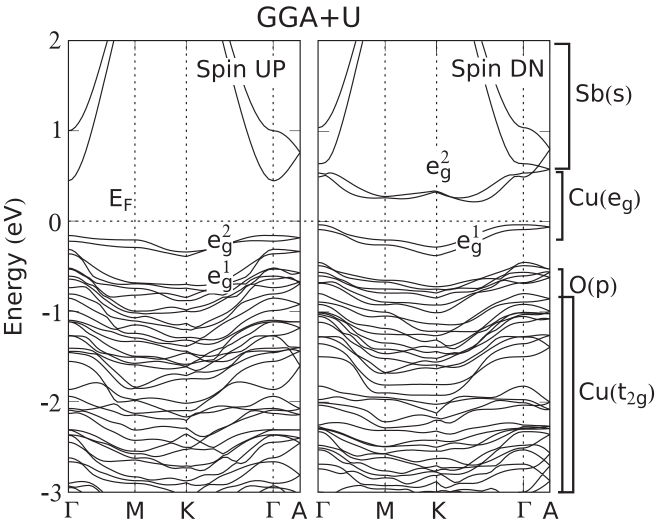

FIG. 8. Same as Fig. 7 but obtained with the GGA+U functional. Here a nonzero JT distortion is present, the magnitude of which was obtained from the structural optimization with the GGA+U functional.

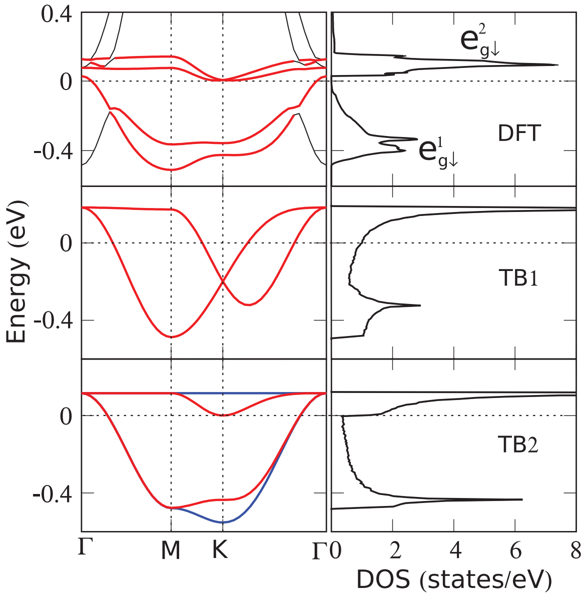

FIG. 9. (Color online) GGA band structure and Cu e_g partial density of states in the minority spin channel for the triangular lattice (top panel). Middle panel shows the results for the simplest TB model [TB1, Eq. (1)] with an effective Cu-Cu hopping between the e_g orbitals, while the bottom panel shows the same for a better TB model [TB2, Eq. (6)], where the effects of oxygen and antimony orbitals were included explicitly via Löwdin downfolding. The e_g orbitals refer to the local axes on each Cu atom as indicated in Fig. 1. There are twice as many e_g bands in the DFT results because the crystal consists of two Cu planes per unit cell, while the TB bands are for one Cu plane. The contributions of the two e_g orbitals ($x^2 - y^2$ and z^2) are the same at every energy in the DOS in the top panel, so that the double-peaked structure does not originate from any JT splitting, but rather from the electronic band structure caused by the particular orientation of the CuO_6 octahedra. The blue lines in the bottom panel indicate bands obtained from the minimal TB2 model with the single parameter V corresponding to the Cu-O-Sb-O-Cu hopping path, which captures the essential features of the e_g bands. The symmetry points are $\Gamma = (0,0)$, $M = (\pi/a)(1,1/\sqrt{3})$, and $K = (2\pi/a)(1/3,1/\sqrt{3})$.

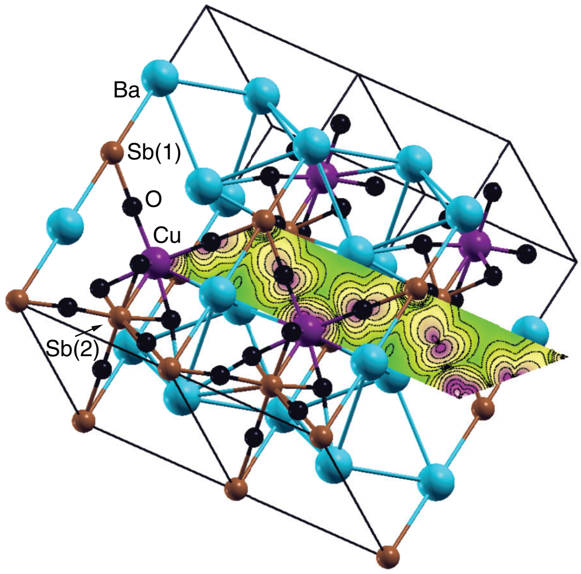

FIG. 10. (Color online) Charge density contours for the Cu (e_g) ↓ hole on a plane containing the hopping paths between the Cu atoms in the triangular structure as obtained from the GGA calculations and plotted on a logarithmic scale. As seen from the partial DOS for Cu ($3d$) and O ($2p$) in Fig. 5, the e_g hole (indicated by $e_g^2\downarrow$ in Fig. 5) has substantial hybridization with the oxygen $2p$ states, which is clearly seen from the charge contours here. Note that the charge density is zero between Cu and O, indicating the expected antibonding Cu-O hybridization for the e_g^2 state. Sb(1) belongs to the Cu-O-Sb-O-Cu hopping path, while Sb(2) makes up the CuO_3Sb dumbbell, which is visible in the figure.

The charge density contours for the $e_g \downarrow$ hole are shown in Fig. 10, where also the electronic hopping paths connecting the Cu-O-Sb-O-Cu atoms have been indicated. The hole has an antibonding hybridization between the Cu (e_g) and the O ($2p$) orbitals, which is visible in the charge-density contours, with a zero charge in the middle of the Cu-O bond.

Tight-binding bands. The simplest tight-binding description (which we refer to as TB1) of the band structure near the Fermi energy is obtained by retaining just two Cu (e_g) orbitals in the Hamiltonian and allowing an effective direct hopping integral between these atoms. That is to say that no oxygen or any other atom is considered in forming this Hamiltonian. However, the e_g orbitals are defined with respect to the local coordinate system, where the coordinate axes on each Cu atom point towards the adjacent oxygen atoms in the CuO_6 octahedra as indicated in Fig. 1. For the triangular structure, there is a single Cu atom in the unit cell and with the standard V_σ and V_π hopping integrals between the d orbitals, the matrix elements of the 2×2 tight-binding Hamiltonian, written in the basis set: $|1\rangle = |x^2 - y^2\rangle$, $|2\rangle = |z^2\rangle$, are given by

$$\begin{aligned} h_{11} &= 2V_\pi \cos 2\eta_x + (3V_\sigma/4 + V_\pi)\cos\eta_x \cos\eta_y, \\ h_{12} &= -\sqrt{3}(V_\sigma/4 - V_\pi)\sin\eta_x \sin\eta_y, \quad h_{21} = h_{12}^*, \\ h_{22} &= V_\sigma/2 \cos 2\eta_x + (V_\sigma/4 + 3V_\pi)\cos\eta_x \cos\eta_y. \end{aligned} \tag{1}$$

This we call the TB1 Hamiltonian. Here $\eta_x \equiv k_x a/2$, $\eta_y \equiv \sqrt{3}k_y a/2$, and a is the distance between two nearest-neighbor Cu atoms on the triangular lattice. The band structure and the DOS obtained from the TB1 Hamiltonian are shown in the middle panel of Fig. 9. A fit to the triangular GGA band structure yields the parameters $V_\sigma = 0.5$ eV and $V_\pi = -0.04$ eV. While this treatment describes the gross features of the band structure including the double peak structure in the DOS, the band dispersion over the Brillouin zone is not very well described. The reason is that the TB hopping occurs via the oxygen atoms, so that the hopping between the Cu (e_g) is the strongest, when the two e_g orbitals are oriented along the respective Cu-O bonds on the two Cu atoms, rather than along the nearest-neighbor Cu-Cu direction, which is the case for TB1.

Löwdin downfolding and the minimal tight-binding Hamiltonian (TB2). To remedy this, a better tight-binding treatment (we call this TB2) is necessary, which explicitly involves the relevant O and Sb orbitals along the hopping path. We obtain a tight-binding Hamiltonian matrix involving all these orbitals and construct an effective 2×2 Hamiltonian in the Cu (e_g) subspace by folding in the effects of the other orbitals via Löwdin downfolding [17]. This is in essence a perturbative method, which works if the energies of the orbitals to be downfolded are far removed from the main orbitals of interest. The Löwdin downfolding procedure for solving the eigenvalue problem $(H - \lambda I)|\psi\rangle = 0$ is to partition the Hamiltonian into blocks:

$$H = \begin{pmatrix} h & b \\ b^\dagger & c \end{pmatrix}, \tag{2}$$

where we are not interested in the higher-energy states in the block c, but include their effects on the block h by perturbation theory. Now, the exact result for the effective Hamiltonian for states in the h subspace is given by

$$h' = h + b(\lambda I - c)^{-1} b^\dagger, \tag{3}$$

which however involves the eigenvalue λ of the full Hamiltonian. It can be shown that an iterative solution of Eq. (3) produces the Brillouin-Wigner perturbation series, which to the lowest order yields the result

$$h'_{ij} = h_{ij} + \sum_k \frac{b_{ik} b_{kj}}{\lambda - c_{kk}}, \tag{4}$$

where i and j belong to the subspace h and k belongs to the subspace c, which is being downfolded.

In most cases λ can be replaced by the diagonal elements h_{ii} and Eq. (4) is valid if $|b_{ik}| \ll |h_{ii} - c_{kk}|$. In the present case, h refers to the Cu (e_g) subspace and with the on-site energy taken as $\varepsilon_d = 0$ and no direct hopping present between the Cu atoms, $h = 0$, so that Eq. (3) leads to the final result $h' = -bc^{-1}b^\dagger$. For a single Cu plane, the planar unit cell has the formula CuO_6SbBa, if we retain the possibility of hopping via the Sb atom as well as via the Ba atom (see Fig. 1), the second being the less important path because of the somewhat larger Ba-O distances. Retaining Cu (e_g), Sb (s), Ba (s), and one O (p_z) (p_z along the Cu-O bond) orbital, we have a full 10×10 Hamiltonian, which is constructed with Harrison's tight-binding matrix elements [18]. After Löwdin downfolding we get the following effective 2×2 Hamiltonian in the Cu (e_g) subspace:

$$h_{\text{eff}} = \begin{pmatrix} h'_{11} & h'_{12} \\ h'_{21} & h'_{22} \end{pmatrix}, \tag{5}$$

where the matrix elements are

$$\begin{aligned} h'_{11} &= -(3V/2)\cos 2\eta_x, \quad h'_{21} = h'^{*}_{12}, \\ h'_{12} &= \sqrt{3}\sin\eta_x[V\sin\eta_y + iV'(\cos\eta_y - \cos\eta_x)], \\ h'_{22} &= (V/2)(\cos 2\eta_x - 4\cos\eta_x\cos\eta_y). \end{aligned} \tag{6}$$

This we call the TB2 Hamiltonian. We propose that this effective 2×2 Hamiltonian together with a Hubbard-U Coulomb interaction term and an appropriate $E \otimes e$ Jahn-Teller coupling term [11,12] [see Eq. (12)] is a minimal model for the description of the electronic structure for the triangular lattice. A somewhat simpler model results if we omit the hopping via the Cu-O-Sb-O-Cu hopping path, in which case we have a single tight-binding parameter $V = V'$, an expression for which is given in Eq. (7).

Note that this Hamiltonian cannot simply be obtained by just retaining the Cu (e_g) orbitals on the triangular lattice and by using the standard tight-binding treatment, which in fact yielded the TB1 matrix discussed earlier, but it must be obtained by the downfolding procedure. We still have just two independent parameters V and V', which can be expressed in terms of the on-site energies and the hopping integrals between the nearest neighbor atoms, viz., ε_p(O), ε_s(Sb), ε'_s(Ba), $V_{pd\sigma}$(O-Cu), $V_{sp\sigma}$(Sb/Ba-O). In terms of these parameters, we have $V = (\alpha_1 + \alpha_2 - \beta)/\Delta$ and $V' = (\alpha_2 - \alpha_1)/\Delta$, where $\alpha_1 = \varepsilon_p \varepsilon_s V^2_{pd\sigma}$, $\alpha_2 = \varepsilon_p \varepsilon'_s V^2_{pd\sigma}$, $\beta = 6V^2_{pd\sigma}V^2_{sp\sigma}$, and $\Delta = 9\varepsilon_p V^2_{sp\sigma} - 3\varepsilon_p^2(\varepsilon_s + \varepsilon'_s) + \varepsilon_p^3 \varepsilon_s \varepsilon'_s V^{-2}_{sp\sigma}$. We have fitted the triangular GGA bands to obtain the two Hamiltonian parameters: $V = -0.15$ eV and $V' = -0.10$ eV. As seen by diagonalizing Eq. (6), the bandwidth in the model is $4|V|$ at the M point and $9|V'|/2$ at the K point in the Brillouin zone.

The tight-binding band structure obtained from the diagonalization of the Hamiltonian (6) is shown as red lines in the bottom panel of Fig. 9, which fits with the DFT bands remarkably well, including the band gap at the K point in the Brillouin zone. Note that the DFT results (top panel) have double the number of Cu (e_g) bands because the unit cell has two copper planes, while the TB model is for just one plane and, furthermore, that the band shown in the top panel as a black line is an Sb (s) band, which is not taken into account in the TB models. In the DFT results, these two bands split by a small amount due to the weak interaction between the two Cu planes, an effect not included in the TB models.

A simpler tight-binding model results if we omit the electron hopping path via the Ba atom, retaining only the dominant Cu-O-Sb-O-Cu hopping path. This can be accomplished by simply taking the Ba on-site energy to be infinity, $\varepsilon'_s \to \infty$, in the TB parameters of Eq. (6), which yields

$$V = V' = \frac{V^2_{pd\sigma}}{\varepsilon_p} \frac{1}{\varepsilon_s \varepsilon_p / V^2_{sp\sigma} - 3}, \tag{7}$$

so that we have just a single TB parameter.

This minimal one-parameter TB2 model indeed captures the essential features of the density-functional e_g bands rather well. In this case, the diagonalization of Eq. (6) yields the eigenvalues

$$\varepsilon_k^{\pm} = \begin{cases} -3V/2, \\ -2V(\cos^2\eta_x + \cos\eta_x\cos\eta_y - 5/4), \end{cases} \tag{8}$$

which are shown as blue lines in the bottom panel of Fig. 9. The above equation shows, quite remarkably, that one of the two bands, in fact the one that makes up the Cu (e_g) hole, is flat over the entire Brillouin zone, if we neglect the weaker hopping path via the Ba atom. This explains the nearly flat band for the Cu (e_g) hole seen in the density-functional bands. This represents the simplest minimal model for the description of the e_g band structure.

B. Band structure for the hexagonal lattice

The hexagonal structure is less symmetric with six Cu atoms in the unit cell, two on each of the two hexagonal planes and two Cu′ atoms out of the plane, which makes a tight-binding description quite complex, but can nevertheless be achieved. The DOS for the hexagonal lattice obtained from the density-functional calculations is shown in Fig. 11

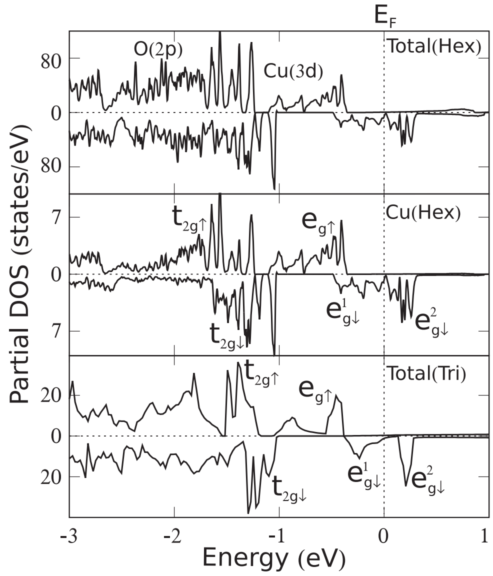

FIG. 11. Spin-polarized electronic densities of states for the hexagonal and the triangular structures obtained from the GGA calculations, indicating the presence of one minority-spin e_g hole ($e_g^2 \downarrow$) in both cases.

and compared with the tight-binding results in Fig. 12. The overall electronic structure is essentially the same as for the triangular structure and we still have the $e_g^2 \downarrow$ hole, except that the presence of the out-of-plane Cu′ atoms leads to a more complicated DOS, with several peaks in the e_g^1 and e_g^2 bands. The essential features of the DOS are captured by the tight-binding Hamiltonian TB1 described earlier, for which the calculated DOS is shown in the bottom panel of Fig. 11.

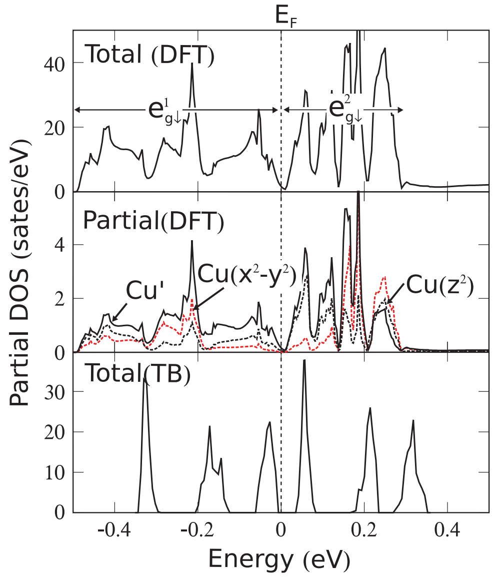

FIG. 12. (Color online) Density of states for the e_g bands in the minority spin channel for the hexagonal structure as obtained from GGA and from the tight-binding TB1 model. The partial DOS in the middle panel is per Cu atom and the figure shows that both the in-plane Cu and out-of-plane Cu′ atoms contribute to the e_g hole (there are six e_g holes now, one per copper atom).

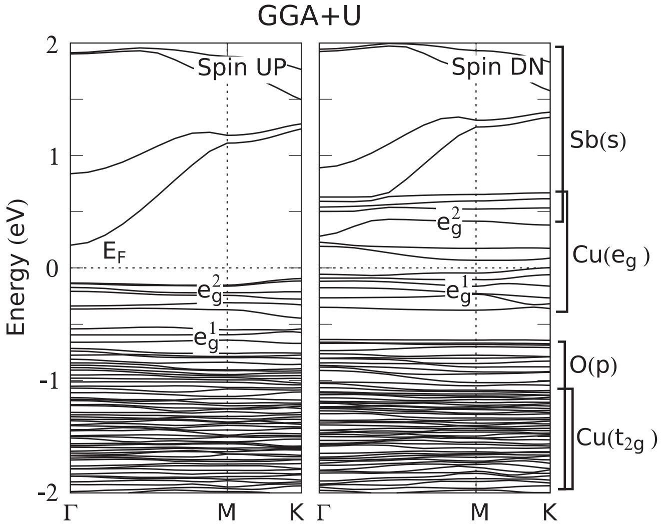

FIG. 13. Spin-polarized GGA+U bands for the hexagonal structure. An insulating solution is obtained and there is one $e_g^2 \downarrow$ hole present per Cu atom.

The better tight-binding Hamiltonian, the TB2, may be easily constructed by keeping the $(CuO_3)_2$ $(Cu'O_3)$ Sb_2 atoms in the minimal model and downfolding it into a 6 × 6 effective Cu (e_g) Hamiltonian following the Löwdin procedure described for the triangular structure. The algebra is straightforward but tedious and it would yield an effective minimal Hamiltonian in the Cu (e_g) subspace for the hexagonal structure.

Figure 13 shows the GGA+U band structure for the hexagonal structure. Since the GGA+U optimization is found to leave Cu, Sb, and Ba positions unchanged in our calculations with triangular structure, we took the relaxed oxygen positions of CuO_6 octahedra from that calculation and applied it to the hexagonal structure with the elongation axis pointing towards the Cu′ position. This structure without further optimization was used for the band structure calculation in Fig. 13.

IV. JAHN-TELLER EFFECT

Even though a strong JT effect might be expected for the Cu (d^9) ion with one hole, no static JT distortion has been observed in the experiment. This has led to the idea that either the JT effect is dynamical [9] or that it is static, but the individual octahedra are randomly oriented with a rather disordered lattice [13,19,20], so that they do not show up in the experimental measurements. Our results suggests a random static JT distortion. We find that while the band structure term suppresses the static JT distortion within the DFT, a finite JT distortion results when the electron correlation effects are taken into account within the DFT+U method. Exact diagonalization studies of a simple model illustrates the correlation-driven Jahn-Teller distortion, which we discuss in Sec. IV B.

A. Large kinetic energy suppresses the JT distortion

1. Two-site model

It is easy to illustrate the adverse effect of the kinetic energy (band structure) term on the JT distortion from a simple two-site model. One intuitively thinks of the JT effect keeping in mind an isolated system such as the CuO$_6$ octahedron. However, as is well known, the electron kinetic energy is also an important consideration for a solid with a lattice of JT centers.

Consider a two-site model with a doubly degenerate orbital at each site occupied by one electron or a hole as relevant for a lattice of Cu (d^9) ions. Since both sites are occupied by one electron each, the kinetic energy gain comes from hopping between the lower level of one atom with energy $-gQ$ to the higher level $E = gQ$ of the second, where the doubly degenerate states at each site are now split due to the JT interaction. This is described by the Hamiltonian $H = \begin{pmatrix} -gQ & t \\ t & gQ \end{pmatrix}$, where t is the intersite hopping integral, g is the linear JT coupling constant, and Q is the magnitude of the JT distortion. By diagonalizing the matrix and adding the elastic energy term, the total energy can then be written as

$$E = (-gQ) + (gQ - \sqrt{t^2 + g^2Q^2}) + 2^{-1}KQ^2, \quad (9)$$

where the three terms in this expression are, respectively, the on-site JT energy gain of the electron, the band structure energy gain E_{bs} due to hopping, and the elastic energy cost. Note that while the first term favors a JT distortion with the gain of energy $-gQ$, the band structure term cancels it in the lowest order of the distortion Q. The band structure energy gain for the electron E_{bs} is the largest when the orbital it is hopping to has the same energy. It readily follows from the above energy expression that the JT distortion occurs only when the JT coupling parameter g is sufficiently strong, so that

$$\lambda_{\rm JT} \equiv g^2/(WK) > \lambda_c, \quad (10)$$

where the critical value turns out to be $\lambda_c = 1/2$ for the two-site model considered here. In the equation above, the bandwidth parameter $W = 2t$ and note that for the isolated site ($W = 0$), the JT distortion occurs no matter how small the magnitude of g is. In other words, all else remaining the same, the bandwidth W must remain below a critical value for the JT distortion to be present in the solid. It is the strength of the dimensionless parameter $\lambda_{\rm JT}$ that controls the magnitude of the JT distortion in the solid. The value of the critical strength λ_c depends on the details of the band structure but it is generally of the order of one, as we found for the two-site model in Eq. (10).

2. *Tight-binding model for the triangular structure with JT coupling*

In order to study the competition between the various terms in the total energy, we have extended the same analysis as above to the solid using the triangular structure. The essential results are true irrespective of the lattice used. The total energy is described by the Hamiltonian

$$\mathcal{H} = \mathcal{H}_{ke} + \mathcal{H}_{\rm JT} + \tfrac{1}{2}KQ^2, \quad (11)$$

where for $\mathcal{H}_{ke}$ we use the tight-binding Hamiltonian Eq. (6), while the second term is the on-site $E \otimes e$ JT interaction term

$$\mathcal{H}_{\rm JT} = -g(Q_2\tau_x + Q_3\tau_z), \quad (12)$$

where g is the linear JT coupling strength, Q_2, Q_3 are the two active octahedral distortion modes, $\vec{\tau}$ is the pseudospin describing the e_g orbitals, $|\uparrow\rangle = |x^2 - y^2\rangle$, and $|\downarrow\rangle = |z^2\rangle$.

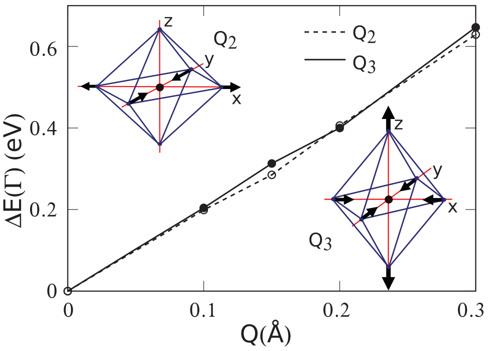

FIG. 14. (Color online) DFT-GGA calculation of the JT coupling strength g, which is obtained from the slope of the energy splitting between e_g^1 and e_g^2 at the Γ point in the triangular structure, viz., $\Delta E = 2gQ$, where $Q = (Q_2^2 + Q_3^2)^{1/2}$. The energy splitting is shown as a function of the amplitude of both the JT modes Q_2 and Q_3.

Finally, the last term in the Hamiltonian (11) is the elastic energy cost of the distortion with $Q^2 = Q_2^2 + Q_3^2$.

DFT calculation of the JT coupling parameters. The JT coupling constant g was evaluated from DFT by distorting the CuO$_6$ octahedra in the triangular structure by a fixed amount and then relaxing the remaining atoms using the GGA functional, and finally by calculating the splitting of the two Cu (e_g) bands at the Γ point in the Brillouin zone. Using Eqs. (8) and (12), the energies of the e_g states at the Γ point are found to be $\varepsilon_\pm(\Gamma) = -3V/2 \pm gQ$ with $Q = (Q_2^2 + Q_3^2)^{1/2}$, so that the splitting at the Γ point is directly proportional to the distortion $\Delta E = 2gQ$. The results are shown in Fig. 14, which follows this linear behavior rather well and yields the value $g = 1.0$ eV/Å. Note that the magnitude of g is significantly strong and typical for the JT systems, although it is a bit smaller than the magnitude in the familiar JT compound LaMnO$_3$ [12]. In addition, as already mentioned, the peculiar electronic hopping in the compound already splits up the e_g states, with equal contribution from the two orbitals, which means that there is not that much energy gain as a result of the JT distortion. Finally, the elastic energy constant K was obtained by distorting the CuO$_6$ octahedra in the unit cell by a fixed amount and then by relaxing the remaining atoms using GGA, which yielded the value $K \approx 15$ eV/Å^2.

Tight-binding energy. With the above Hamiltonian parameters, we now examine the contributions of the different parts of the Hamiltonian (11) to the total energy. Figure 15 illustrates the various parts, viz., $E_{\rm elastic} = 1/2KQ^2$, $E_{\rm JT} = -gQ$, and the band structure energy E_{bs}. Note that in this figure the parameters are such that the band structure term is relatively small, so that there is a JT distortion Q present corresponding to the minimum of the total energy $E_{\rm tot}$ indicated by a black dot. Notice also that the band structure energy increases as a function of the JT distortion, so that it does not favor a JT distortion, which is similar to the effect of the elastic energy term. The JT coupling energy $-gQ$ must overcome both the band structure and the elastic energy for the JT distortion to be possible and this is indeed the case in Fig. 15.

However, unlike the case of the isolated octahedron, a JT distortion may not occur at all if g is small. In Fig. 16 we show the total energy for several values of $\lambda_{\rm JT} \equiv g^2/(WK)$. We find that a critical value of $\lambda_{\rm JT} > \lambda_c \approx 0.50$ is needed

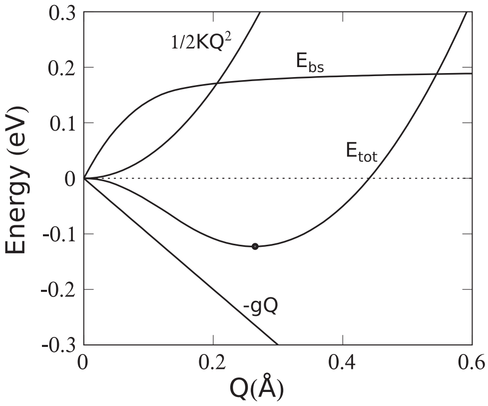

FIG. 15. Illustration of the various components of the energy as a function of the JT distortion obtained for the triangular structure with the Hamiltonian (11). Here the strength of the JT coupling g is large enough to overcome the band structure energy resulting in a JT distortion corresponding to the minimum total energy indicated by the black dot. The parameters here are such that $g^2/(WK) = 1$.

for the existence of a JT distortion of the system, while λ_{JT} is only about $\approx$0.22 in the compound under study, where we used the bandwidth $W = 4|V| \approx 0.6$ eV obtained from the DFT bands. The small value of λ_{JT} for the present compound means that the band structure term overwhelms the JT interaction, characterized by the energy g^2/K, so that there is no JT distortion in the compound. This conclusion is directly supported by the density-functional total energy shown in the same figure as a function of the JT distortion Q, where the lattice is relaxed in each case while keeping the distortion fixed. The DFT curve almost exactly overlaps with the tight-binding curve with $\lambda_{JT} = 0.22$ (not shown in the figure), indicating that the tight-binding model we have employed for the study of the JT effect is quite reasonable.

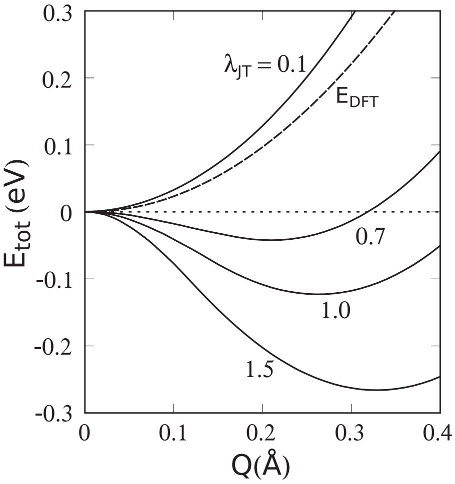

FIG. 16. Variation of the total energy with the distortion Q for several values of the JT coupling strength $\lambda_{JT} = g^2/(WK)$ obtained from Eq. (11) with $\mathcal{H}_{ke}$ described by the TB2 Hamiltonian Eq. (6). The dashed line indicates the DFT-GGA total energy per $Ba_3CuSb_2O_9$ formula unit for the triangular structure obtained by optimizing the crystal structure for each Q; no Jahn-Teller distortion is predicted from the GGA.

B. Correlation driven Jahn-Teller effect in the solid

In the above analysis, correlation effects were not included. Electron correlation effects will, quite generally, enhance the tendency for a JT distortion in the solid, simply because it reduces the kinetic energy of the electrons as they must move in a correlated fashion. The reduction of the kinetic energy due to correlation is quite well known. For example, in the Gutzwiller treatment of correlated systems, the kinetic energy reduction factor may be explicitly evaluated for certain models such as the Hubbard model [21–24]. The kinetic energy becomes smaller and smaller as the strength of the Coulomb interaction is increased and it eventually becomes zero beyond the Brinkman-Rice metal-insulator transition [25]. As is clear from the discussion of the previous subsection, since the kinetic energy suppresses the tendency towards a JT distortion, a reduction of it through correlation will favor a JT distortion.

Exact diagonalization of a model many-body system. To illustrate the above point that correlation diminishes the kinetic energy and hence increases the tendency towards a JT distortion, we consider a simple, exactly solvable model Hamiltonian, viz., a spinless Hamiltonian for a single hexagon of Cu atoms with two orbitals per site with both a Jahn-Teller as well as a Coulomb interaction term present. We have a half-filled system with one electron per site. An exact diagonalization of the many-body Hamiltonian using the Lanczos method yields the ground state energy and allows us to study the Jahn-Teller distortion of the system in the presence of the Coulomb interaction.

The model Hamiltonian reads

$$\mathcal{H} = t \sum_{\langle ij\rangle,\alpha} (c_{i\alpha}^\dagger c_{j\alpha} + \text{H.c.}) + t' \sum_{\langle ij\rangle} (c_{i1}^\dagger c_{j2} + c_{i2}^\dagger c_{j1}) + \text{H.c.} + \sum_i \left[U\, n_{i1} n_{i2} - gQ\,(n_{i1} - n_{i2}) + \frac{1}{2} K Q^2 \right], \quad (13)$$

where $c_{i\alpha}^\dagger$ creates an electron at the ith site in the jth orbital ($i = 1,2,\ldots,6$ and $j = 1,2$), t and t' are the nearest-neighbor hopping integrals, U is the on-site Coulomb interaction, g represents the Jahn-Teller coupling term, Q is the Jahn-Teller distortion of the local site (assumed to be the same on all six sites for simplicity), K is the elastic energy cost of the distortion, and finally $\langle ij\rangle$ denotes the summation over distinct pairs of nearest-neighbor bonds. We take the parameters $t = -0.1$ eV, $t' = 0.05$ eV (which yield a bandwidth of $W = 0.6$ eV in the absence of all other terms), $U = 2$ eV, $g = 1$ eV/Å, and $K = 5$ eV/Å^2. The Hamiltonian was solved exactly by Lanczos diagonalization and also in the Hartree-Fock approximation.

The results are shown in Fig. 17, which beautifully illustrates the essential physics of, what we may call, the correlation-driven JT effect. For the isolated site ($t = t' = 0$), any value of the JT interaction g will produce a distortion $Q = g/K$, which minimizes the total energy expression $E = -gQ + 1/2KQ^2$. However, in the solid, the bandwidth W must remain below a critical value [see Eq. (10) for the two-site model] for the JT distortion to continue when the solid forms. As Fig. 17 indicates, the bandwidth is sufficiently large so as to suppress any JT distortion for the case $U = 0$ eV. When the Coulomb interaction is added ($U = 2$ eV), the electrons

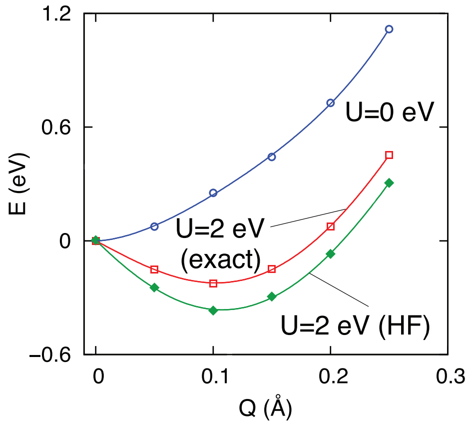

FIG. 17. (Color online) Illustration of the correlation driven Jahn-Teller effect. The figure shows the exact diagonalization results for the Hamiltonian Eq. (13) showing the ground-state energy E as a function of the JT distortion Q. The energy minimum occurs at a nonzero Q if Coulomb interaction is present, while there is no JT distortion ($Q = 0$) for the noninteracting system. Obviously, if $U = 0$, both exact results and the Hartree-Fock results coincide (blue line), since we have a noninteracting system. The energy zeros have been shifted here; the actual exact energies (zero unshifted) are always below the Hartree-Fock energies, since the Hartree-Fock energies are variational estimates of the exact energies.

move in a correlated fashion, in effect, reducing the kinetic energy or the bandwidth, so that the parameter $\lambda_{\mathrm{JT}} \equiv g^2/WK$ exceeds the critical value λ_c, producing a nonzero JT distortion as a result. In the model study, the exact results are mimicked by the Hartree-Fock treatment, but as seen from the figure, the latter yields a somewhat larger JT energy, defined as the energy gained due to the JT distortion.

C. GGA+*U* density-functional results for $\mathrm{Ba_3CuSb_2O_9}$

Within the density-functional method, the correlation effect may be included in an approximate way with the Coulomb-corrected GGA+U functional. The total energy calculations, especially the lattice relaxation from the DFT forces, become quite tedious for a complex crystal structure, so we performed the structural relaxation for the triangular lattice using the GGA+U method. The environment of the in-plane Cu atoms are expected to be more or less the same in both the triangular and the hexagonal structures; so no major differences are expected for the JT distortion of the $\mathrm{CuO_6}$ octahedra between the two structures.

The results for the Cu-O bond lengths obtained from this structural optimization are shown in Fig. 18. Without the Coulomb term ($U = 0$ eV), there is a strong trigonal distortion with three bond lengths (along Cu-O-Ba; see Fig. 1) significantly longer than the three along Cu-O-Sb1. When the Coulomb interaction is included (typical values of $U \approx 4$–8 eV), we find a JT-type distorted octahedron, though the Cu-O bond lengths are stretched by different amounts along $+\hat{z}$ and $-\hat{z}$ directions. The remaining bond lengths are nearly the same. For the triangular structure, the three direction along Cu-O-Sb for this octahedral stretching are identical, thus producing three equivalent JT minima, while for the hexagonal structure, these three directions are not all the same. For the latter case, there is a unique direction defined by joining Cu to Cu′ along Cu-O-Sb1-O-Cu′, which forms a straight line, identifiable in Fig. 3. The other two directions along Cu-O-Sb1 terminate on Sb1. Thus in the hexagonal structure, the three JT minima are not equivalent and one of them will have a different energy than the other two.

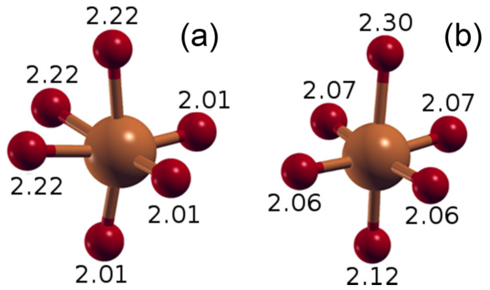

FIG. 18. (Color online) Cu-O bond lengths in the $\mathrm{CuO_6}$ octahedra obtained from the full structural relaxation of the triangular structure with (a) GGA and (b) GGA+U ($U = 4$ eV). The latter shows a JT distortion of the Q_3 type, which is the octahedral stretching mode. In (a), the longer bonds are along Cu-O-Ba, while the shorter bonds are along Cu-O-Sb. Similarly, in (b), the 2.23 Å bond is along Cu-O-Ba, while the 2.12 Å bond is along Cu-O-Sb.

In Fig. 19 we show the total energy with a fixed lattice distortion Q to examine in more detail the energy reduction as a function of the JT distortion. In these calculations we added a fixed Q_3 distortion to the $\mathrm{CuO_6}$ octahedra by displacing the oxygen atoms, fixed the positions of these atoms, and relaxed the remaining structure from the DFT forces. We have taken the value $U = 4$ eV in the GGA+U calculation, which is reasonable for Cu. The results show that the Coulomb interaction term clearly favors a JT distortion as anticipated from the exact diagonalization results for the model system in the previous section (see Fig. 17). Again, the basic physics is that the Coulomb interaction term makes the electrons move

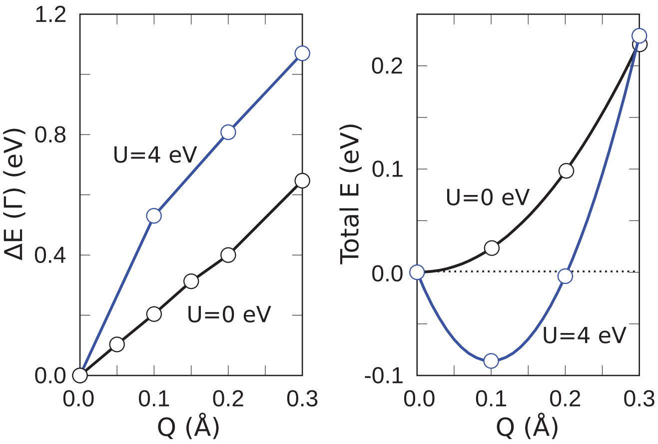

FIG. 19. (Color online) GGA+U total energy E per unit cell (containing two Cu atoms) as a function of the lattice distortion Q, which was held fixed while relaxing the remaining atoms (*right*) and the corresponding gap ΔE between the occupied e_g^1 and the unoccupied e_g^2 state at the Γ point in the Brillouin zone (*left*).

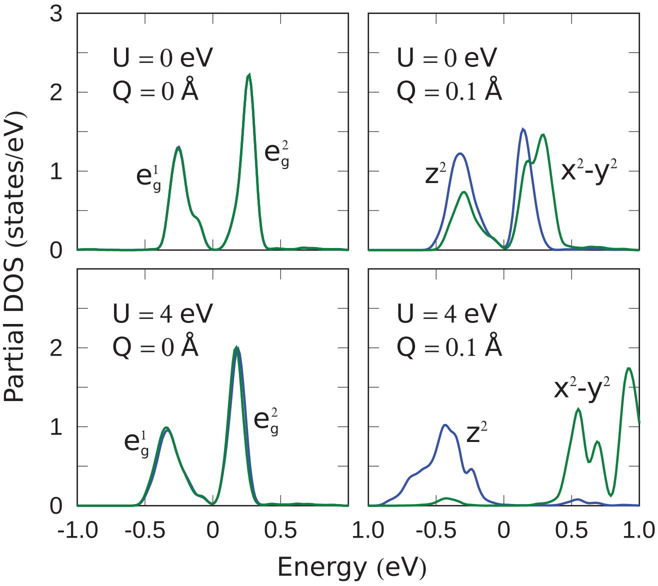

FIG. 20. (Color online) GGA+U results for the densities of states for the minority-spin e_g orbitals. The bottom right panel corresponds to the minimum-energy structure as obtained from the GGA+U total energy, Fig. 19.

in a correlated manner, effectively reducing the kinetic energy due to correlation, with a reduced kinetic energy (or enhanced g^2/WK) favoring the tendency towards the JT distortion. We find from the figure that there is a JT distortion of about $Q = 0.1$ Å, when the Coulomb interaction is included within the GGA+U method.

Figure 20 shows the densities of states for different values of U and the octahedral distortion Q. The results indicate an insulating band gap between the two e_g states, which is also seen from the corresponding band structure, shown in Fig. 8. This insulating behavior is in agreement with experiments.

D. Static vs dynamical JT effect

It is a subject of current debate regarding whether the JT effect in $Ba_3CuSb_2O_9$ is static or dynamical or if there is even any JT effect at all. The original experiments of Köhl [7] measured no noticeable JT distortion of the CuO_6 octahedra. This could however mean that (a) the JT distortions are static but with distortion axes of different octahedra randomly oriented in the crystal (random static JT), so that one measures zero average distortion, or (b) the JT distortions are dynamical, in which case the nuclear framework tunnels between several equivalent minima. We argue below for the random static JT distortion for the hexagonal structure.

First consider the triangular lattice. For this lattice, the three axial (x,y,z) directions along the Cu-O bonds are equivalent, which leads to three equivalent minima of identical energy in the JT problem. For the $E \otimes e$ JT coupling, involving the e_g states and the Q_2, Q_3 modes, the adiabatic potential surface is given by the expression [11]

$$E_\pm = \tfrac{1}{2} K Q^2 \pm Q\sqrt{g^2 + G^2 Q^2 + 2gGQ\cos(3\phi)}, \qquad (14)$$

where $Q = \sqrt{Q_2^2 + Q_3^2}$ and $\phi = \tan^{-1}(Q_2/Q_3)$ are the polar coordinates and $E_\pm$ denote the two potential sheets. Looking at the lower adiabatic potential surface (APS), there are three equivalent minima at $\phi = 0$, $2\pi/3$, and $4\pi/3$, separated by a tunneling barrier between adjacent minima of height $\beta = 2GQ_0^2$, where Q_0 is the location of the minima. From the GGA+U results of Fig. 19, we can estimate the magnitudes of the parameters from the slopes and curvatures of ΔE and the total energy, which yield the values $g \approx 1.3$ eV/Å and $K \approx 15$ eV/Å^2. If we take the minimum of Q from the fully optimized structure [Fig. 18(b)], we find $Q_0 = (Q_2^2 + Q_3^2)^{1/2} \approx Q_3 \approx 0.17$ Å, Q_2 being nearly zero. The parameter G may be indirectly obtained from the expression $Q_0 = g(K - 2G)^{-1}$, which yields the value of the warping parameter $G \approx 3.5$ eV/Å^2, which is rather large (compare this to ∼2 eV/Å^2 for the manganites [12], where the JT distortion is known to be static, and ∼0.4 eV/Å^2 for graphene, where the JT distortion is predicted to be dynamical [26]).

The nuclear tunneling amplitude between the two minima of the APS may be estimated [26] from the expression $T \approx -\Delta V \times F$, where $\Delta V = (\pi^2/2 - 2)Q_0^2 G$ is the deviation of the barrier energy from the ideal simple-harmonic potential of the APS minima and the Frank-Condon factor $F = \int \phi_1^*(R)\phi_2(R)d^3R$ is the overlap between the zero-point nuclear wave functions localized at the neighboring APS minima. This yields the rough tunneling amplitude of $T \approx -13$ meV. A more accurate estimate may be obtained from solving the quantum-mechanical Schrödinger equation for the combined nuclear-electronic motion [26]. This yields the tunneling amplitude of $T \approx -7$ meV. Due to the Berry phase introduced by the motion of the electron that follows the nuclear motion adiabatically, the ground state is doubly degenerate separated from the singly degenerate first excited state by an energy $3|T|$ (21 meV in the present case) in the combined nuclear-electronic problem. This so called tunneling splitting energy is large enough (large as compared to the typical strain splitting of the three JT APS minima, which is typically 5–10 meV) that this would suggest a dynamical JT effect for the triangular lattice.

Turning now to the hexagonal lattice structure, the three JT minima in the APS are no longer equivalent, since the three cubic directions are different owing to the presence of the Cu′ atoms, which results in the unique $\hat{z}$ axis pointed along the Cu-O-Sb-O-Cu′ as seen from the structure figure (Fig. 3). We computed the energies of the three minima for the hexagonal structure from DFT, which shows that one of the three minima (the one that corresponds to Q_3 distortion along the unique $\hat{z}$ axis) has the lower energy than the other two by a large amount of about 43 meV (see Fig. 21). Since the tunneling splitting (estimated to be 21 meV for the triangular structure and will be even smaller for the hexagonal structure, since the three minima have unequal energies now) is significantly less than the 43 meV, the system will have a static JT distortion corresponding to this minimum. Now, the Cu′ atoms come from the inversion of the Cu-Sb dumbbells; so if these flipped dumbbells are disordered as suggested from the experiments, then the most favorable JT minimum with Q_3 along $\hat{z}$ also changes from one CuO_6 octahedron to another, leading to the random static JT distortions, a scenario that is

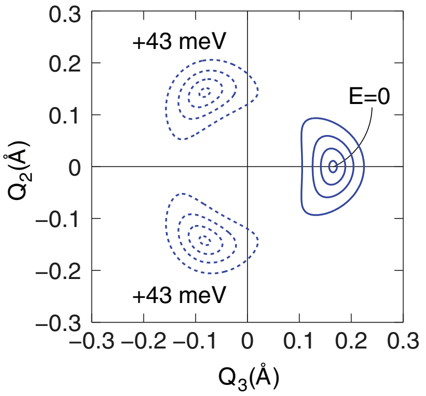

FIG. 21. (Color online) Illustration of the energy contours of the lower APS for the $E \otimes e$ Jahn-Teller effect. For the triangular structure, the three minima are all equivalent and have the same energy [Eq. (14)]. However, for the hexagonal structure, one of the three minima, shown as solid contours here, which occurs along the Q_3 direction with the z axis defined in Fig. 3, has a lower energy (by about 43 meV according to the GGA+U calculations) as compared to the other two minima.

favored by some experiments [19]. In essence, the significantly smaller tunneling splitting is unable to overcome the large energy difference between the three minima in the hexagonal structure, thus suggesting the presence of the random JT distortions.

On the other hand, if the three JT minima are close in energy, as our calculations suggest for the triangular structure, then Nasu and Ishihara [9] have recently proposed that the dynamical JT effect would lead to the correlation between spin and orbital motion. Recent experiments [27] on the hexagonal material have found evidence for such spin-orbital correlation, but our work suggests that the dynamical JT effect is unlikely to be the reason behind it.

V. SUMMARY

In summary, we studied the electronic structure of the spin liquid candidate $Ba_3CuSb_2O_9$ from density-functional methods both in the triangular and the hexagonal lattice structures. Electron states near the Fermi energy are well described in terms of the Cu (d^9) with a single e_g hole in both the structures. A Löwdin procedure was used to obtain a minimal tight-binding Hamiltonian model for the Cu (e_g) bands by downfolding the oxygen p orbitals and an expression for this Hamiltonian was given explicitly for the triangular lattice [Eq. (5)]. A similar minimal Hamiltonian may be obtained for the hexagonal structure as well.

We studied the presence of the JT effect in the compound from structural energy minimization within the Coulomb-corrected GGA+U method and found that the correlation effects are important for the JT distortions of the CuO_6 octahedra. First, we illustrated the idea of the correlation-driven JT effect by the exact diagonalization of a simple tight-binding model Hamiltonian on a hexagon (Sec. IV B). These results are quite generally applicable and not just limited to the present system under study. The basic point is that correlation effects enhance the tendency towards the JT distortion by reducing the bandwidth W, e.g., via the Gutzwiller bandwidth reduction factor, which then enhances the strength of the effective JT parameter $\lambda_{\rm JT} = g^2/WK$ responsible for the JT distortions in the solid. For the present compound, we found no JT distortions within the density-functional calculations, while inclusion of the Coulomb correlation effects within the GGA+U method yielded significant JT distortions.

Regarding the nature of the JT distortions, we examined whether they are random static distortions or dynamical JT distortions. For the triangular structure, the three minima of the APS are equivalent from symmetry. Based on the JT parameters estimated from the GGA+U functional, we obtained a significant magnitude for the nuclear tunneling splitting ($3|T| \approx 21$ meV) due to the quantum mechanical nuclear motion between these three minima, which signaled a dynamical JT effect because this splitting is much higher than the typical strain splitting of 5–10 meV in the solid. However, for the hexagonal structure, the environment of the octahedra has broken spatial symmetry, so that the three energy minima of the APS are no longer equivalent. GGA+U results showed that one of the three minima (Fig. 21) is lower than the other two by as much as 43 meV. Because this is significantly larger than the tunneling splitting, our results suggest a static JT effect for the hexagonal structure. The JT distortions are furthermore expected to be random because of the presence of disordered Cu-Sb flipped dumbbells and other disorder in the system.

ACKNOWLEDGMENT

This work was supported by the U. S. Department of Energy through Grant No. DE-FG02-00ER45818.

---

[1] R. Moessner and A. Ramirez, Phys. Today **59**, 24 (2006).
[2] L. Balents, Nature (London) **464**, 199 (2010).
[3] A. P. Ramirez, A. Hayashi, R. J. Cava, R. Siddharthan, and B. S. Shastry, Nature (London) **399**, 333 (1999).
[4] L. Pauling, *The Nature of the Chemical Bond* (Cornell University Press, Ithaca, NY, 1960).
[5] W. F. Giauque and J. W. Stout, J. Am. Chem. Soc. **58**, 1144 (1936).
[6] P. W. Anderson, Mater. Res. Bull. **8**, 153 (1973).
[7] V. P. Köhl, Z. Anorg. Allg. Chem. **442**, 280 (1978).
[8] H. D. Zhou, E. S. Choi, G. Li, L. Balicas, C. R. Wiebe, Y. Qiu, J. R. D. Copley, and J. S. Gardner, Phys. Rev. Lett. **106**, 147204 (2011).
[9] J. Nasu and S. Ishihara, Phys. Rev. B **88**, 094408 (2013).
[10] C. Broholm (private communication).
[11] I. B. Bersuker, *The Jahn-Teller Effect* (Cambridge University Press, Cambridge, 2006).
[12] Z. S. Popović and S. Satpathy, Phys. Rev. Lett. **84**, 1603 (2000).
[13] S. Nakatsuji, K. Kuga, K. Kimura, R. Satake, N. Katayama, E. Nishibori, H. Sawa, R. Ishii, M. Hagiwara, F. Bridges,

T. U. Ito, W. Higemoto, Y. Karaki, M. Halim, A. A. Nugroho, J. A. Rodriguez-Rivera, M. A. Green, and C. Broholm, Science **336**, 559 (2012).

[14] G. Kresse and J. Hafner, Phys. Rev. B **47**, 558 (1993); G. Kresse and J. Furthmuller, *ibid.* **54**, 11169 (1996).

[15] J. P. Perdew, K. Burke, and Y. Wang, Phys. Rev. B **54**, 16533 (1996).

[16] V. I. Anisimov, J. Zaanen, and O. K. Andersen, Phys. Rev. B **44**, 943 (1991).

[17] P. Löwdin, J. Chem. Phys. **19**, 1396 (1951).

[18] W. A. Harrison, *Electronic Structure and the Properties of Solids* (Freeman, San Francisco, 1980).

[19] J. A. Quilliam, F. Bert, E. Kermarrec, C. Payen, C. Guillot-Deudon, P. Bonville, C. Baines, H. Luetkens, and P. Mendels, Phys. Rev. Lett. **109**, 117203 (2012).

[20] L. Balents, Science **336**, 547 (2012).

[21] M. C. Gutzwiller, Phys. Rev. Lett. **10**, 159 (1963).

[22] M. C. Gutzwiller, Phys. Rev. **137**, A1726 (1965).

[23] M. Sherafati, S. Satpathy, and D. Pettey, Phys. Rev. B **88**, 035114 (2013).

[24] See, for example, D. Vollhardt, Rev. Mod. Phys. **56**, 99 (1984); F. Gebhard, *The Mott Metal-Insulator Transition* (Springer, Berlin, 1997).

[25] W. F. Brinkman and T. M. Rice, Phys. Rev. B **2**, 4302 (1970).

[26] Z. S. Popović, B. R. K. Nanda, and S. Satpathy, Phys. Rev. B **86**, 085458 (2012).

[27] Y. Ishiguro, K. Kimura, S. Nakatsuji, S. Tsutsui, A. Baron, T. Kimura, and Y. Wakabayashi, Nat. Commun. **4**, 2022 (2013).